

## Article

# Friction and Wear Properties of Silicon Nitride-Based Composites with Different hBN Content Sliding against Polyether-Etherketone at Different Speeds under Artificial Seawater Lubrication

Huaqiang Li <sup>1</sup>, Xingwei Liu <sup>1</sup>, Chen Zhang <sup>1</sup>, Xiaoyu Jiao <sup>2</sup>, Wei Chen <sup>2,\*</sup>, Jinghui Gao <sup>1</sup> and Lisheng Zhong <sup>1,\*</sup>

<sup>1</sup> State Key Laboratory of Electrical Insulation and Power Equipment, Xi'an Jiaotong University, Xi'an 710049, China; lhqxjtu@xjtu.edu.cn (H.L.); lxw2018@stu.xjtu.edu.cn (X.L.); zc.zgp.gy@stu.xjtu.edu.cn (C.Z.); gaojinghui@xjtu.edu.cn (J.G.)

<sup>2</sup> College of Mechanical and Electrical Engineering, Shaanxi University of Science & Technology, Xi'an 710021, China; 1905008@sust.edu.cn

\* Correspondence: chenweijd@sust.edu.cn (W.C.); lszhong@xjtu.edu.cn (L.Z.)

**Abstract:** In the present study, the friction and wear behaviors of Si<sub>3</sub>N<sub>4</sub>-hBN (Hexagonal boron nitride) ceramic composites against polyether-etherketone in artificial seawater were investigated, and the sliding speed was varied from 0.52 to 1.73 m/s to study the effect. It was found that the friction coefficients and wear rates decreased with the increase in sliding speed for Si<sub>3</sub>N<sub>4</sub>-hBN (with the hBN content ranging from 5% to 20%) against PEEK (Polyether-ether-ketone); the sliding pairs represented an upward trend as the speed increased for Si<sub>3</sub>N<sub>4</sub>-hBN (with an hBN content of 0 and 30%) against PEEK. This result was mainly attributed to complex friction resistance sources, such as mechanical meshing and the shear strength of soft tribofilm. On the other hand, both the hBN content and sliding speed had a significant effect on the tribological performance of the Si<sub>3</sub>N<sub>4</sub>-hBN/PEEK pairs. Meanwhile, the lowest friction coefficient of 0.07 and wear rates below 10<sup>-6</sup> mm<sup>3</sup>/Nm were obtained from the Si<sub>3</sub>N<sub>4</sub>-20%hBN/PEEK pair at the speed of 1.73 m/s.

**Keywords:** silicon nitride; tribofilm; sliding speed; mechanical meshing



**Citation:** Li, H.; Liu, X.; Zhang, C.; Jiao, X.; Chen, W.; Gao, J.; Zhong, L. Friction and Wear Properties of Silicon Nitride-Based Composites with Different hBN Content Sliding against Polyether-Etherketone at Different Speeds under Artificial Seawater Lubrication. *Coatings* **2022**, *12*, 411. <https://doi.org/10.3390/coatings12030411>

Academic Editor: Joel Rech

Received: 13 February 2022

Accepted: 8 March 2022

Published: 19 March 2022

**Publisher's Note:** MDPI stays neutral with regard to jurisdictional claims in published maps and institutional affiliations.



**Copyright:** © 2022 by the authors. Licensee MDPI, Basel, Switzerland. This article is an open access article distributed under the terms and conditions of the Creative Commons Attribution (CC BY) license (<https://creativecommons.org/licenses/by/4.0/>).

## 1. Introduction

The vast ocean is not only the cradle of life on Earth, but also a treasure house of resources that have not been fully exploited [1,2]. With the depletion of terrestrial energy, marine energy has become the world's new preferred energy source. However, marine equipment is subjected to harsh operational conditions, and the wear fault of the power systems is, thus, prominent. The key friction pairs in marine installations (e.g., seawater plunger pumps) often undergo severe corrosion and wear during the service process, which seriously limits the reliability and service life of the marine equipment [3–6]. As a result, further improving the tribological properties of marine friction pairs is an urgent task [7,8].

Ceramic materials are known for their outstanding hardness, high strength, excellent chemical stability, and corrosion resistance compared with traditional metal pairs, which make them promising candidates for marine friction pairs. In this respect, more and more scholars are paying attention to the tribological performance of ceramics in marine environments [9–11]. In particular, silicon nitride can react with water molecules during the friction process to form silica gel, which, afterwards, transforms into a surface lubricating film on the wear surface [12–15]. Meanwhile, Liu [16] investigated the tribological properties of single-phase Si<sub>3</sub>N<sub>4</sub> sliding against stainless steel in water and seawater, and observed an increase in the friction coefficients and wear rates of the friction pair. Similarly, Zhang [17] analyzed the tribological characteristics of a titanium–zirconium–molybdenum alloy sliding against single-phase Si<sub>3</sub>N<sub>4</sub> in seawater, where the tribochemical products had

difficulty aggregating into the film, which resulted in a higher friction coefficient in the friction pair. Wang [18] also investigated the tribological performance of single-phase  $\text{Si}_3\text{N}_4$  sliding against a Cr/GLC film in seawater, successfully obtaining better friction and wear properties. Nevertheless, even the excellent performance of the film could not provide continuous lubrication, thus facing the problems associated with lubrication and protection. Therefore, there is an urgent need to develop silicon nitride-based ceramics with improved tribological properties that would withstand severe marine conditions.

Among the reliable ways to enhance the tribological performances of such composites is adding a solid lubricant, hBN, to a silicon nitride ceramic matrix. For example, Skopp and Carrapichano [19,20] have shown that embedding hBN allows one to improve the tribological characteristics of single-phase  $\text{Si}_3\text{N}_4$  to various extents. Moreover, our research team [21,22] has also shown that the incorporation of hBN into  $\text{Si}_3\text{N}_4$  is beneficial to the friction and wear properties of ceramics, which is due to the release of the tribochemical products of hBN and  $\text{Si}_3\text{N}_4$  with water molecules. In addition, Cho [23] has also found that a higher hBN content in  $\text{Si}_3\text{N}_4$ -hBN composites results in slower R-curves, which could enhance the micro-machinability. As can be observed from the existing literature, there are not enough systematic studies focused on the tribological properties of  $\text{Si}_3\text{N}_4$ -hBN ceramics exposed to marine environments, which limits the research and exploration of this composite material in marine equipment.

Based on what is described above, it is of great significance to further study the tribological behavior of  $\text{Si}_3\text{N}_4$ -hBN composite materials in a marine environment. In the present study, the tribological performance of the  $\text{Si}_3\text{N}_4$ -hBN composite at different speeds was assessed in artificial seawater, through an upper pin-on-bottom disc test. One special plastic polyether-etherketone (PEEK) was selected as the mating material, because of its great potential in the field of engineering tribology and marine equipment [24–26]. The wear mechanism is further explored by measuring the friction coefficient and wear rate, observing worn morphology, analyzing the chemical composition of the tribofilm, and combining analysis with classical theory.

## 2. Experimental Procedures

### 2.1. Preparation of Specimens

Commercial  $\alpha$ - $\text{Si}_3\text{N}_4$  powder with a mean size of 0.40–0.60  $\mu\text{m}$  and 99.99% purity was used to conduct this investigation. hBN powder with a mean size of 0.3  $\mu\text{m}$  and 99.8% purity was used as the second additive phase. Oxide additives of  $\text{Y}_2\text{O}_3$  and  $\text{Al}_2\text{O}_3$  (mean size of 1  $\mu\text{m}$  and >99.5 purity) were used as sintering aids. Powders were mixed by ball mill (KQM-X4Z/B, Xianyang, China) at 500 rpm for 5 h with zirconia balls to a powder ratio of 2:1 in alcohol for 24 h. After the slurry was dried, the mixed powders were utilized in five  $\text{Si}_3\text{N}_4$ -hBN composites with 0%, 5%, 10%, 20% and 30% hBN (named as SN0, SN5, SN10, SN20 and SN30) by hot-press sinter of 30 MPa in flowing  $\text{N}_2$  at 1800 °C for 30 min in an graphite die. Disc specimens with a size of  $\Phi 44 \text{ mm} \times 6 \text{ mm}$  were then produced. The XRD results of the sintered specimens for  $\text{Si}_3\text{N}_4$  and  $\text{Si}_3\text{N}_4$ -30%hBN are shown in Figure 1, and it can be observed that the pure  $\text{Si}_3\text{N}_4$  specimen is composed of  $\beta$ - $\text{Si}_3\text{N}_4$ , and that the ceramic composite is composed of  $\beta$ - $\text{Si}_3\text{N}_4$  and hBN. Thus, it can be concluded that the  $\alpha$ - $\text{Si}_3\text{N}_4$  raw powder has been completely transformed to  $\beta$ - $\text{Si}_3\text{N}_4$  during the sintering process, and that the hBN powder did not undergo any phase transformation. So, the composite ceramics were composed of  $\beta$ - $\text{Si}_3\text{N}_4$  columnar crystal and hBN sheets. The physical and mechanical properties of the ceramic composites are shown in Table 1, revealing a downtrend in the mechanical performance with the increase in hBN content.

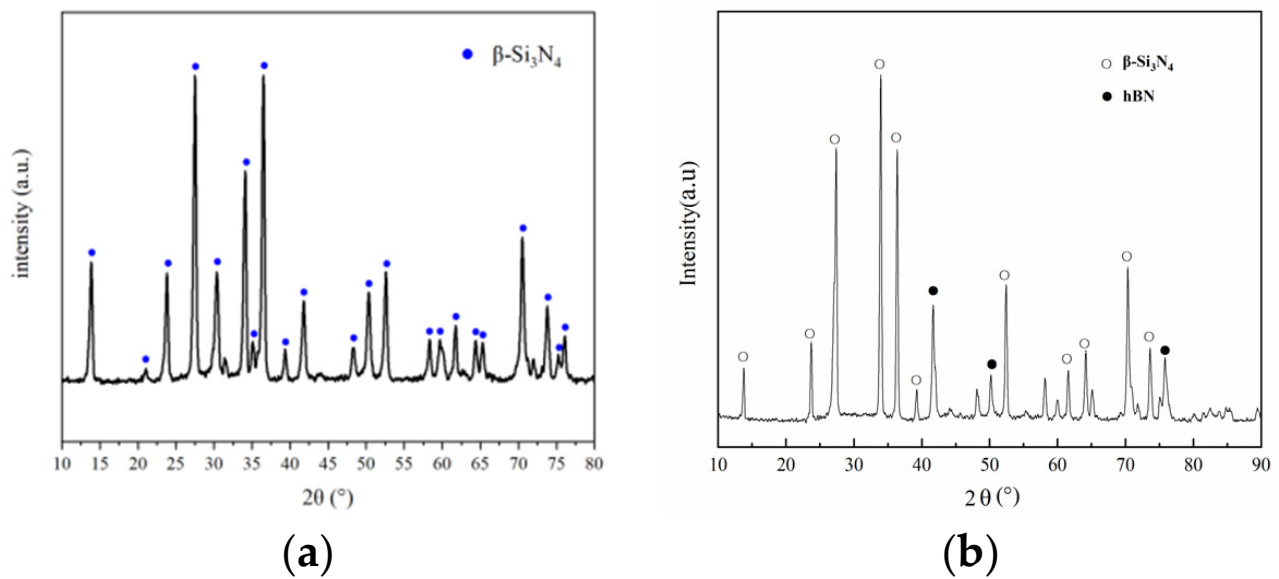


**Figure 1.** XRD analysis results of (a) SN0 and (b) SN30 specimens.

**Table 1.** Physical and mechanical properties of specimens [27].

Specimens	hBN Amount (wt.%)	Density (g/cm <sup>3</sup> )	Porosity (%)	Bending Strength (MPa)	Vickers Hardness (GPa)	Fracture Toughness (MPa·m <sup>1/2</sup> )
SN0	0	3.31	0.84	812	19.9	8.01
SN5	5	3.17	0.90	758	19.6	7.80
SN10	10	3.10	0.91	613	15.3	7.14
SN20	20	2.97	1.04	541	9.3	5.97
SN30	30	2.94	1.05	465	6.7	5.50

The as-sintered ceramic composite samples (with a size of  $\Phi 45 \text{ mm} \times 5 \text{ mm}$ ) were machined into pins for friction and wear tests. The pin samples with a size of  $5 \text{ mm} \times 5 \text{ mm} \times 15 \text{ mm}$  were cut from the  $\text{Si}_3\text{N}_4$ -based materials using a diamond wheel. The pin surfaces were polished, using a diamond grinding tool, down to a surface roughness below  $\text{Ra}0.08 \text{ }\mu\text{m}$ . The disc samples with a dimension of  $\Phi 44 \text{ mm} \times 6 \text{ mm}$  were made from commercial PEEK bars, and the disc samples were polished down to surface roughness below  $\text{Ra}0.04 \text{ }\mu\text{m}$ . All the pin and disc samples were dried after ultrasonic cleaning for the wear test.

## 2.2. Procedure

Sliding wear tests were carried out on a MMW-1 pin-on-disc wear tester (made by Jinan Zhongchuang Industrial Test System Co., Ltd., Jinan, China). In this tester, an upper pin contacts a stationary disc when artificial water is supplied to the contact surface, and the wear interfaces are fully immersed in the seawater, as shown in Figure 2. Meanwhile, the artificial seawater (whose salinity is 35 g/L) was prepared according to Standard ASTM D 1141-98.

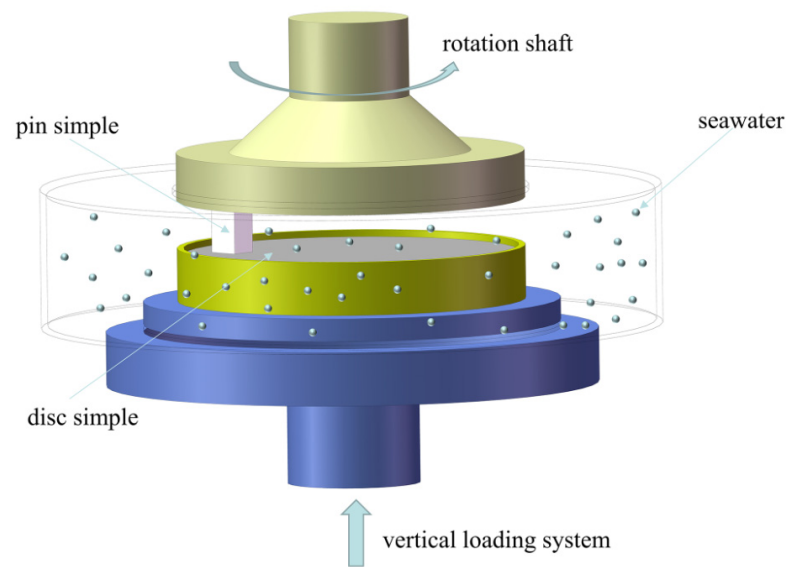


**Figure 2.** Schematic diagram of a pin-on-disc tester.

The wear tests were performed in artificial seawater under a normal load of 20 N and at room temperature. While loaded, the pin samples rotated at the speeds of 300 rpm (0.52 m/s), 500 rpm (0.86 m/s), and 1000 rpm (1.73 m/s). Every test was run over a period of 2010 m. The initial running-in period was not accounted for in the calculation of friction coefficient and wear rate in the steady state of friction. The friction coefficient  $f$  was directly estimated by the tester. The wear rate  $k$  was calculated from the formula  $k = \Delta m / \rho P d$ , where  $\Delta m$  (mg) is the mass wear loss, measured with a microbalance with an accuracy of 0.1 mg,  $P$  (N) is the normal load,  $d$  (m) is the sliding distance, and  $\rho$  (g/cm<sup>3</sup>) is the density.

Three tribological tests were carried out three times under the same conditions. The masses of pins and discs were gauged before and after each measurement. In such a setting, the average friction coefficients and wear rates were obtained from the test data. The morphology and chemical composition of the specimens of the worn surface were examined via scanning electron microscopy (SEM, FEI Q45, Hillsboro, OR, USA) and energy dispersive spectroscopy (EDS, FEI, Hillsboro, OR, USA). The corresponding composition of the compound was detected via X-ray photoelectron spectroscopy (XPS, K-Alpha, Waltham, MA, USA).

### 3. Results and Discussion

Figure 3 displays the friction coefficients and wear rates of the Si<sub>3</sub>N<sub>4</sub>-hBN/PEEK sliding pairs at different speeds in artificial seawater. It can be observed from Figure 3a that the sliding speed exerts a significant effect on the friction coefficient, which is, however, different for Si<sub>3</sub>N<sub>4</sub> ceramics with various hBN contents. In particular, the friction coefficients of the Si<sub>3</sub>N<sub>4</sub>-hBN/PEEK pairs decrease with the increase in sliding speed, when the hBN content is in the range from 5% to 20%. Meanwhile, the friction coefficient increases with increasing sliding speed for the SN0/PEEK and SN30/PEEK pairs. Among these sliding pairs, the lowest friction coefficient of 0.07 was obtained at a speed of 1.73 m/s for the SN20/PEEK pair. The corresponding wear rates of the pins and discs present a similar change law (see Figure 3b,c). Meanwhile, all of the wear rates of the pins and discs were less than 10<sup>-6</sup> mm<sup>3</sup>/Nm orders of magnitude. In general, the SN20/PEEK pair presented the best tribological properties at a sliding speed of 1.73 m/s, and Figure 4 shows the change curves of the friction coefficients of the SN20/PEEK pair at different sliding speeds.

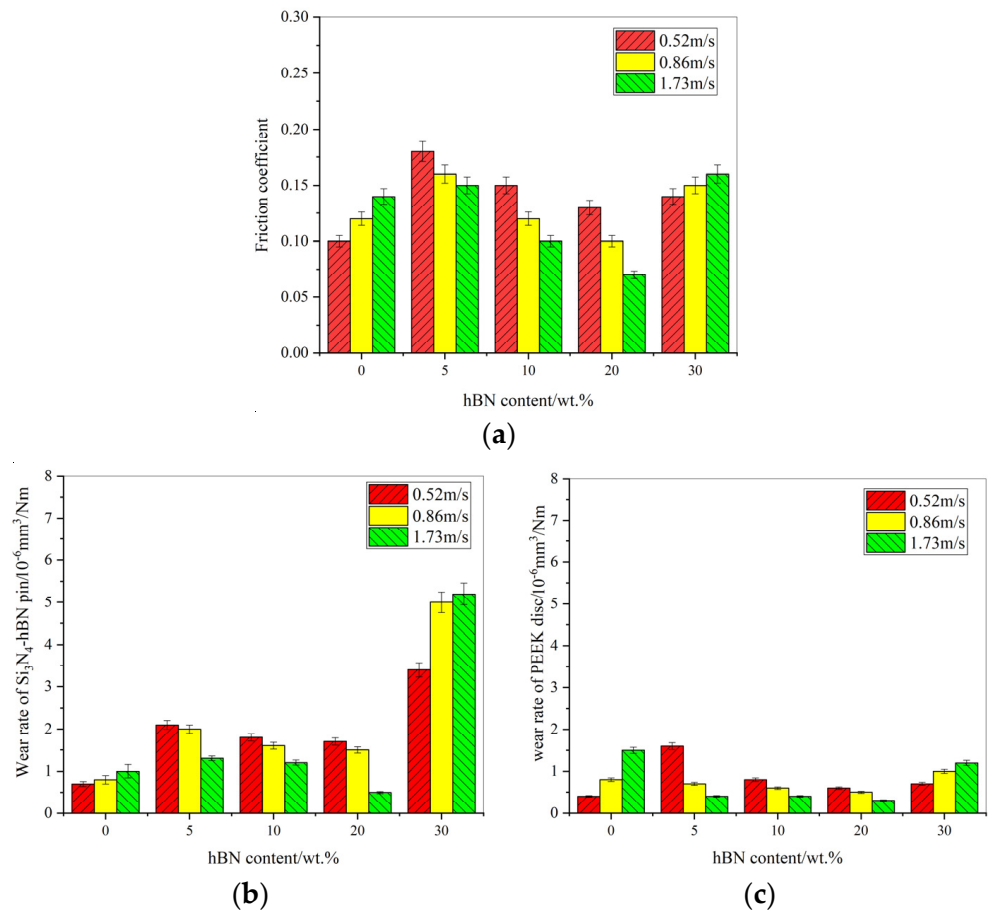


**Figure 3.** Friction coefficients and wear rates of Si<sub>3</sub>N<sub>4</sub>-hBN/PEEK pairs in artificial seawater: (a) friction coefficients; (b) wear rates of pins; (c) wear rates of discs.

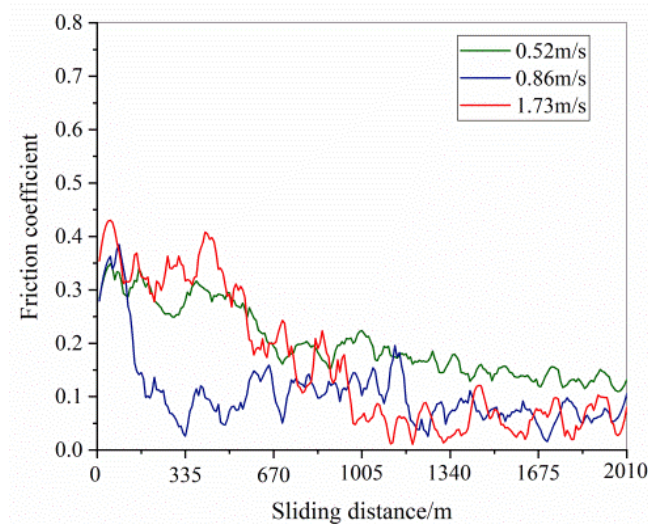


**Figure 4.** The change curves of the friction coefficients of SN20/PEEK as a function of friction distance.

Figure 5 shows the morphologies of the worn surfaces of the PEEK discs sliding against the SN20 pin at the different sliding speeds in seawater. The worn surface of the PEEK disc gradually became smooth with increasing speed. Some wear particles and squamous broken morphologies were observed on the worn surface of the PEEK disc at the speed of 0.52 m/s (Figure 5a). A pronounced furrow morphology was observed on

the worn surface of the PEEK disc at the speed of 0.86 m/s (Figure 5b). At the speed of 1.73 m/s, a very smooth worn surface can be observed on the PEEK disc (Figure 5c).

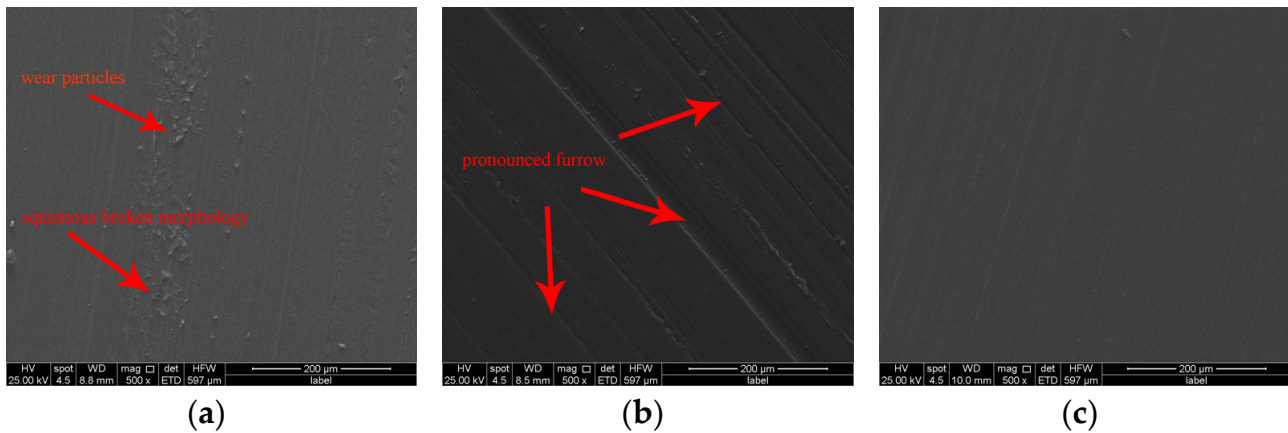


**Figure 5.** SEM images of worn surface of the PEEK disc against the SN20 pin at the following different speeds in artificial seawater: (a) 0.52 m/s; (b) 0.86 m/s; (c) 1.73 m/s.

Figure 6 shows the morphologies of the worn surface of the SN20 pin at different sliding speeds in seawater. Plenty of spalling pits and cracks are clearly visible on the worn surface of the SN20 pin at the speed of 0.52 m/s (Figure 6a). At the speed of 0.86 m/s, the worn surface of the SN20 pin is covered with furrows (Figure 6b). A further increase in the speed, to 1.73 m/s, leads to the emergence of smooth black areas and rough areas on the worn surface (Figure 6c). Meanwhile, detached material and abrasions can be observed on the edges of the smooth areas and rough regions. The EDS spectrum of the smooth black area (indicated with arrows in Figure 6c) reveals the presence of Si, O, Ca, and Mg elements (as shown in Figure 7). The B element was not detected because its low weight is beyond the measuring capabilities of the EDS technique. Moreover, the Mg and Ca elements should be from the seawater.

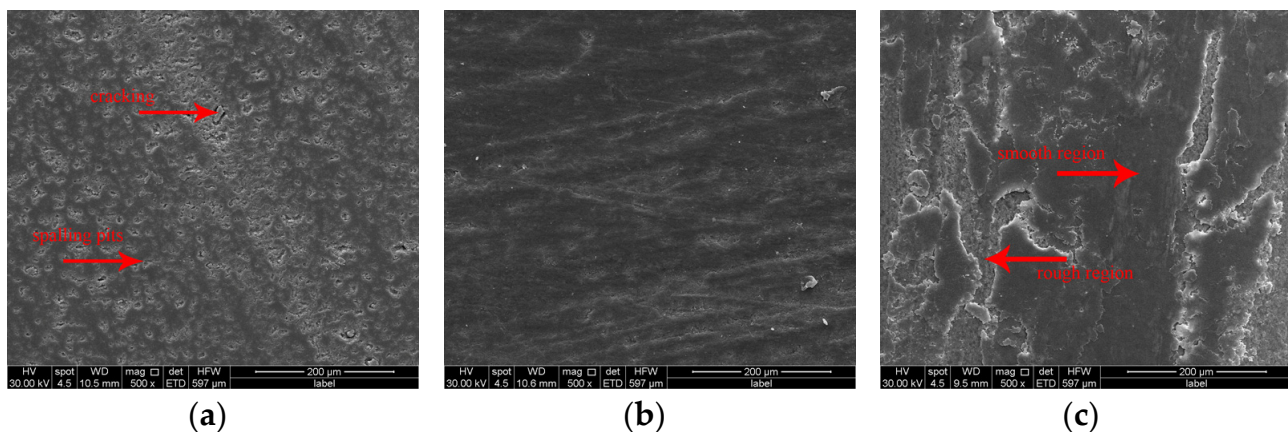


**Figure 6.** SEM images of worn surfaces of the SN20 pins at the following different speeds in artificial seawater: (a) 0.52 m/s; (b) 0.86 m/s; (c) 1.73 m/s.

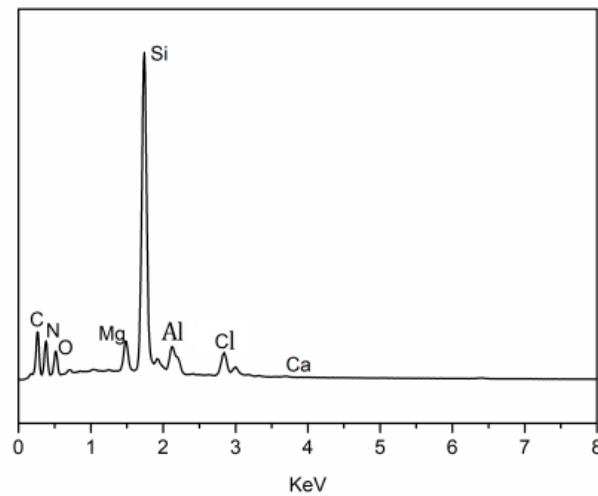


**Figure 7.** EDS spectrum of the black area on the worn surface of the SN20 pin against the PEEK disc at the speed of 1.73 m/s.

Figure 8 displays the XPS spectra with the Si2p and B1s peaks, which are acquired on the worn surface of the SN20 pin against the PEEK disc at the speed of 1.73 m/s in artificial seawater. Through the fitting curve method, the Si2p peak was decomposed into the following two peaks: one at 101.8 eV, corresponding to  $\text{Si}_3\text{N}_4$ , and another at 103.4 eV, corresponding to  $\text{SiO}_2$  (Figure 8a). Meanwhile, the B1s peak was decomposed into two peaks at 190.2 and 190.5 eV (Figure 8b), which were associated with BN and  $\text{B}_2\text{O}_3$ , respectively. Meanwhile, the XPS results also show the presence of magnesium and calcium oxides, or hydroxides. These data coincide with those from our previous study [21,28], wherein some tribochemical products composed of  $\text{SiO}_2$ ,  $\text{B}_2\text{O}_3$ , the metal oxides and hydroxides, were detected on the wear surface of the  $\text{Si}_3\text{N}_4$ -hBN composite after the friction process. Combined with the EDS analysis results and our previous work [29], we can conclude that some tribochemical products (indicated by arrows in Figure 5c) formed on the wear surface of the SN20 pin against the PEEK disc, and the tribochemical products aggregated into the black surface film.

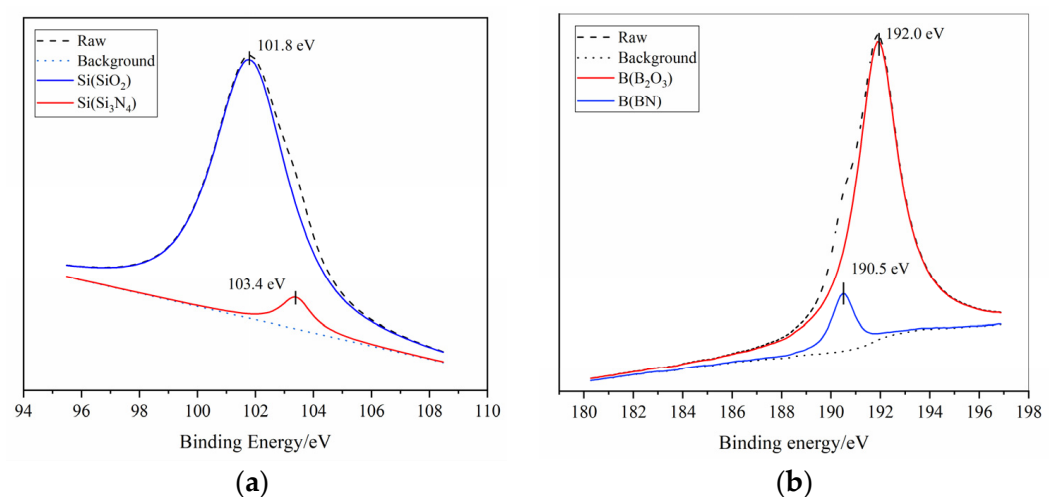


**Figure 8.** XPS spectra of the worn surface of the SN20 pin against the PEEK disc in artificial seawater: (a) Si2p; (b) B1s.

In this study, when the SN20 pin slid against the PEEK disc at a speed of 1.73 m/s, the hard ceramic micro-bulge damaged the PEEK surfaces at the initial stage of the friction process, resulting in the formation of spalling pits and, consequently, the wear particles

(which generally came from the hBN agglomeration area of the pin surface). One part of the wear particles was carried away from the wear interface by the seawater, and some wear particles could be reacted with the seawater, contributing to the formation of tribochemical products (enough tribochemical reaction products could aggregate to form a surface film). In this case, the wear surface covered with black film was in direct contact, and another part of the wear interface was filled with seawater.

According to the binomial law of friction [30], sliding friction is the process of overcoming the mechanical meshing of surface micro-convex and molecular attraction, so friction is the combination of mechanical and molecular resistance, namely, the following:

$$F = \tau_0 S_0 + \tau_m S_m \quad (1)$$

where  $S_0$  and  $S_m$  are the areas of molecular attraction and mechanical meshing, respectively.  $\tau(0)$  and  $\tau(m)$  are the forces of friction caused by the molecular attraction and mechanical meshing per unit area, respectively.

Therefore, for the SN20/PEEK pair at the speed of 1.73 m/s, the mechanical meshing areas ( $S_m$ ) of this sliding pair approached zero, and the friction forces were mainly from the molecular attraction. Meanwhile, the molecular attraction force originated from the resistance of the seawater and the shear strength of the surface film, namely, the following:

$$F \approx \tau_0 S_0 = \tau_f S_f + \tau_l S_l \quad (2)$$

where  $S_f$  and  $S_l$  are the area of surface film contact and the area filled with seawater, respectively.  $\tau(f)$  and  $\tau(l)$  are the shear strength of the surface film and the seawater resistance per unit area, respectively.

As we know, the seawater's resistance at the wear interface is very small, namely,  $\tau_l \rightarrow 0$ . So, Equation (2) becomes the following equation:

$$F \approx \tau_f S_f \quad (3)$$

According to our previous study [31], the surface film containing  $\text{SiO}_2$ , B–O compound, and some alkali metal oxide possessed low shear strength and an excellent antifriction effect, namely, the shear strength of the tribofilm ( $\tau_f$ ) should be very low. The lower friction coefficient of 0.07 was, therefore, obtained for the sliding pair of SN20/PEEK at the speed of 1.73 m/s.

In addition, under the condition of seawater lubrication, a decrease in the sliding speed was expected to trigger a reduction in the flash temperature of the wear surface (which was not conducive to tribochemical reactions), and to cause the wear particles to easily remain in the wear interface (which led to abrasive wear and promoted mechanical meshing). Figure 9 depicts enlarged images revealing the surface morphologies of the SN20 pins at the speed of 0.52 m/s. It can be clearly observed that some loose wear particles implant in the spalling pits, and that not all the debris was eliminated by the seawater. In such a setting, Equation (1) becomes the following equation:

$$F \approx \tau_f S_f + \tau_m S_m \quad (4)$$

So, with the decrease in sliding speed, the friction coefficient of the SN20/PEEK pair increased. Meanwhile, due to more drastic mechanical meshing, the wear rate also continued to rise, as shown in Figure 9.

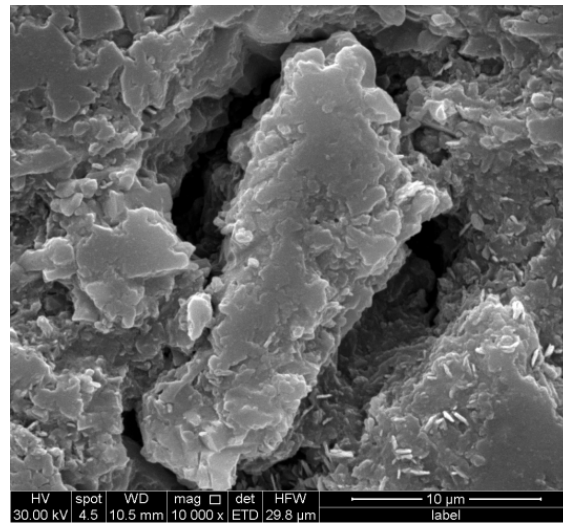


**Figure 9.** Enlarged image of the surface morphology of SN20 pins at the speed of 0.52 m/s.

When the SN5 and SN10 pins slide against the PEEK disc in seawater, the variation in friction and wear behavior with speed is similar to that of the SN20/PEEK pair. Rough worn surfaces of the SN10 and SN5 pins at a speed of 0.52 m/s can be observed, as shown in Figures 10a and 11a, while the relatively smooth surfaces at a speed of 1.73 m/s can be clearly observed in Figures 10b and 11b. So, for these pairs, the increase in speed promoted the progress of tribochemical reactions and inhibited the degree of mechanical meshing. However, when the hBN content reached 30 wt.%, serious degradation of the mechanical properties led to a very rough wear surface during the friction process. In this case, the mechanical meshing was unavoidable, even when the friction pair was cooled and lubricated by seawater, so friction is the combination of mechanical meshing and molecular resistance. Thus, the friction coefficients of the SN30/PEEK pair were higher than those of SN20/PEEK. Moreover, an increase in speed aggravated the fracture and spalling of the ceramic pins and mechanical meshing, so the friction coefficient and wear rate of the SN30/PEEK pair increased with increasing speed.

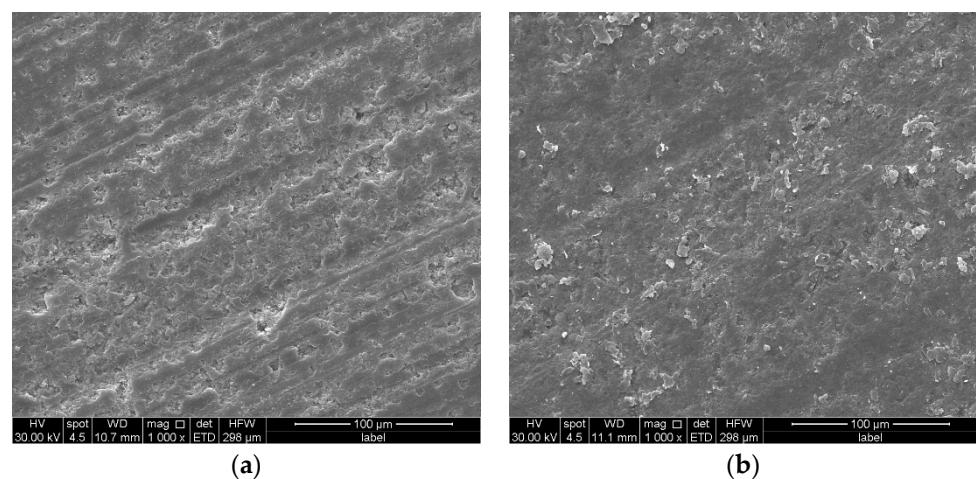


**Figure 10.** Worn surfaces of the SN10 pin against the PEEK disc in artificial seawater at the following different speeds: (a) 0.52 m/s; (b) 1.73 m/s.

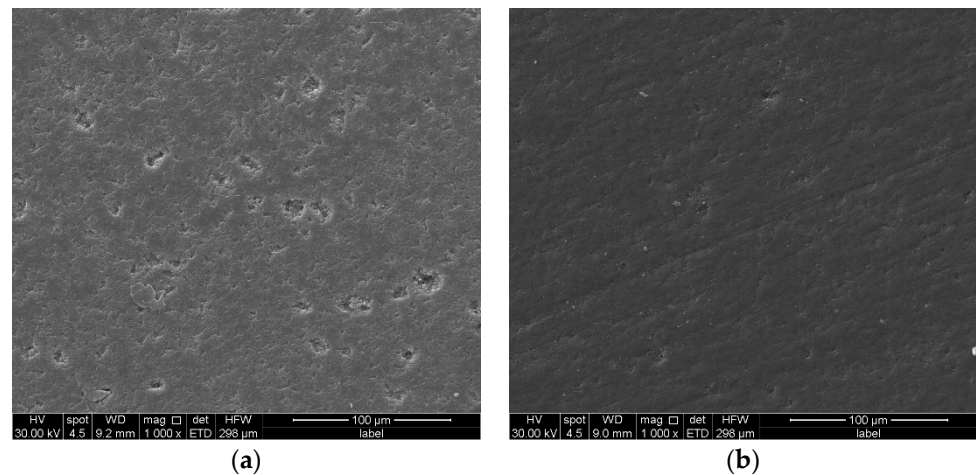


**Figure 11.** Worn surfaces of the SN5 pin against the PEEK disc in artificial seawater at the following different speeds: (a) 0.52 m/s; (b) 1.73 m/s.

When the SN0 pin slid against the PEEK disc, the morphologies of the worn surfaces for the SN0 pin are shown in Figure 12. No obvious tribofilm is observed on the worn surface, and some spalling pits formed on the worn surfaces of the SN0 pin at the sliding speeds of 0.52 and 1.73 m/s. Meanwhile, there are fewer, but larger, spalling pits on the worn surface at the speed of 0.52 m/s (Figure 12a), while there are much more and smaller spalling pits on the worn surface at the speed of 1.73 m/s (Figure 12b). The rough surfaces suggest that mechanical meshing occurs on the wear surface when the SN0 pin slides against the PEEK disc, and is not avoided by the lubrication of seawater and the generation of tribochemical products (e.g.,  $\text{SiO}_2$ ). Figure 13 shows the morphology of the worn surface of the PEEK disc at the speed of 1.73 m/s, revealing the furrow, trivial peeling off, and tiny particles. So, the higher friction coefficient of the SN0/PEEK pair was in the range of 0.1 to 0.22. Meanwhile, with the increase in speed, the frequent plowing and mechanical meshing resulted in a greater friction coefficient and a higher wear rate.

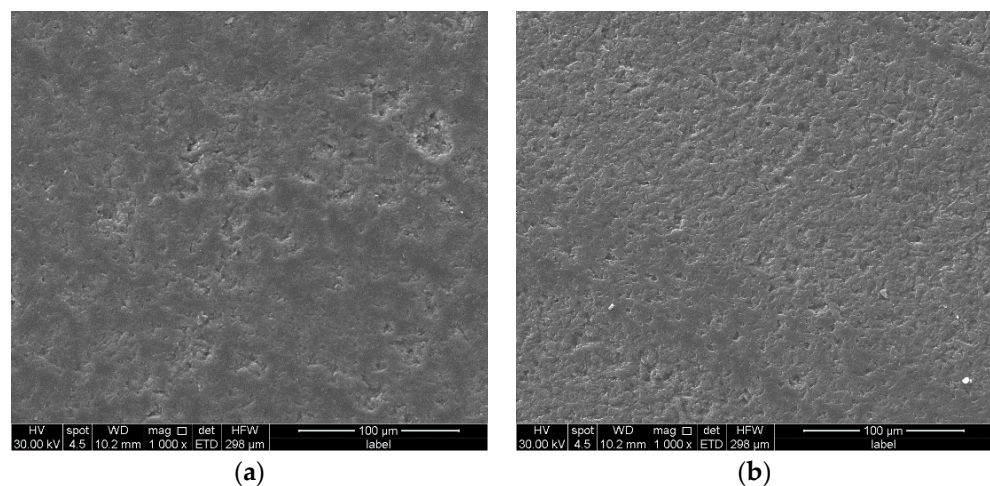


**Figure 12.** Worn surfaces of the SN0 pin against the PEEK disc in artificial seawater at the following different speeds: (a) 0.52 m/s; (b) 1.73 m/s.

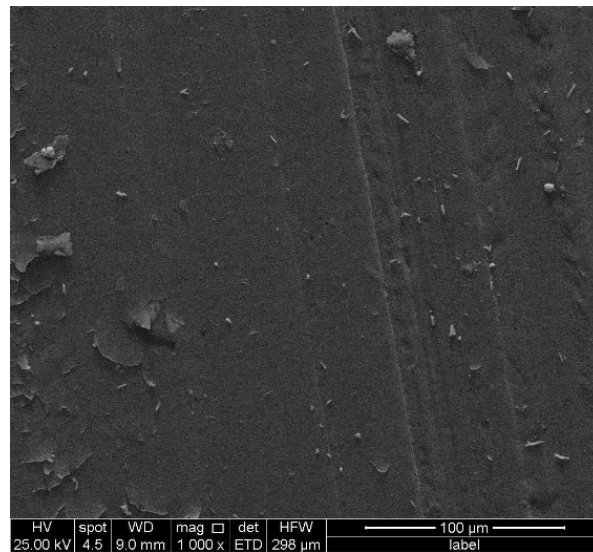


**Figure 13.** SEM image of the worn surface for the PEEK disc against the SN0 pin at the speed of 1.73 m/s.

In summary, the incorporation of hBN into a silicon nitride matrix reduced the mechanical properties, but provided conditions for the formation of a tribofilm. When the content of hexagonal boron nitride was in the range of 5% to 20%, the friction caused by mechanical meshing could be weakened by the formation of the tribofilm. As the speed increased, more wear debris was taken away from the wear interface, and the tribofilm was more continuously formed on the wear surface. So, the sliding pairs presented lower and lower friction and wear with the increase in speed. When the hBN content reached 30%, severe deterioration of the mechanical properties caused an extremely rough wear surface with more serious mechanical wear. Once the speed increased, the mechanical wear became more severe under the action of shear force. Hence, the friction coefficient and wear rate of the SN30/PEEK pair increased with the increase in the sliding speed. When the SN0 pin slid against the PEEK disc, no tribofilm formed on the worn surface, and the main source of friction force came from mechanical meshing. Meanwhile, the increase in speed aggravated the frequent plowing and mechanical meshing, resulting in a greater friction coefficient and a higher wear rate.

#### 4. Conclusions

Based on the results of the present work, the following conclusions can be drawn:

1. Under an artificial seawater environment, the friction and wear performance of Si<sub>3</sub>N<sub>4</sub>-hBN/PEEK pairs was affected by the sliding speed. With the hBN content increased from 5% to 20%, the friction coefficients and wear rates decreased with the increase in sliding speed. With hBN contents of 0 and 30%, the sliding pairs represented an upward trend as the speed increased. Meanwhile, the lowest friction coefficient of 0.07 and wear rates below the magnitude of 10<sup>-6</sup> mm<sup>3</sup>/Nm were obtained for the SN20/PEEK pair at a sliding speed of 1.73 m/s.
2. When the SN20 pin slid against the PEEK disc, the tribofilm was gradually formed on the wear surface in seawater, which was mainly due to the higher flash temperature and less wear debris produced by the increase in speed. When the friction resistance of the sliding pair mainly came from the shear strength of soft tribofilm, the sliding pair entered a state of low friction and wear.
3. When the SN0 pin slid against the PEEK disc, no tribofilm formed on the wear surfaces, and part of the friction resistance was from the mechanical meshing, resulting in higher friction and wear. Simultaneously, the increase in speed aggravated the frequent plowing and mechanical meshing. For the SN30/PEEK pair, severe deterioration of the mechanical properties caused an extremely rough wear surface with more serious

mechanical wear. Once the speed increased, the mechanical meshing became more severe under the action of shear force.

**Author Contributions:** Conceptualization, H.L.; Data curation, X.L., C.Z. and X.J.; Investigation, X.L., C.Z. and X.J.; Methodology, J.G.; Project administration, W.C.; Supervision, H.L. and L.Z.; Writing—original draft, W.C.; Writing—review & editing, H.L. All authors have read and agreed to the published version of the manuscript.

**Funding:** This research was funded by Natural Science Foundation of Shaanxi Province, China (Grant No. 2018JM5056).

**Institutional Review Board Statement:** Not applicable.

**Informed Consent Statement:** Not applicable.

**Data Availability Statement:** Not applicable.

**Conflicts of Interest:** The authors declare no conflict of interest.

## References

- Zhao, J.; Han, B.; Cui, G.; Zhang, S.; Li, M.; Wang, Y. Preparation of Ni55 + FeS composite coatings and their antifriction performances in artificial seawater. *Mater. Des.* **2017**, *131*, 375–383. [\[CrossRef\]](#)
- Haq, M.I.U.; Raina, A.; Vohra, K.; Kumar, R.; Anand, A. An Assessment of Tribological Characteristics of Different Materials under Sea Water Environment. *Mater. Today Proc.* **2018**, *5*, 3602–3609. [\[CrossRef\]](#)
- Ma, F.; Li, J.; Zeng, Z.; Gao, Y. Structural, mechanical and tribocorrosion behavior in artificial seawater of CrN/AlN nanomultilayer coatings in F690 steel substrates. *Appl. Surf. Sci.* **2018**, *428*, 404–414. [\[CrossRef\]](#)
- Liu, X.; Zhao, X.; An, Y.; Hou, G.; Li, S.; Deng, W.; Zhou, H.; Chen, J. Effects of loads on corrosion-wear synergism of NiCoCrAlYTa coating in artificial seawater. *Tribol. Int.* **2018**, *118*, 421–431. [\[CrossRef\]](#)
- Ye, Y.; Wang, Y.; Ma, X.; Zhang, D.; Wang, L.; Li, X. Tribocorrosion behaviors of multilayer PVD DLC coated 304L stainless steel in seawater. *Diam. Relat. Mater.* **2017**, *79*, 70–78. [\[CrossRef\]](#)
- John, M.; Menezes, P.L. Self-Lubricating Materials for Extreme Condition Applications. *Materials* **2021**, *14*, 5588. [\[CrossRef\]](#)
- Cai, Y.; Yin, X.; Fan, S.; Zhang, L.; Cheng, L. Tribological behavior of three-dimensional needled ceramic modified carbon/carbon composites in seawater conditions. *Compos. Sci. Technol.* **2013**, *87*, 50–57. [\[CrossRef\]](#)
- Zhang, Y.; Yin, X.-Y.; Yan, F.-Y. Tribocorrosion behavior of type S31254 steel in seawater: Identification of corrosion-wear components and effect of potential. *Mater. Chem. Phys.* **2016**, *179*, 273–281. [\[CrossRef\]](#)
- Chen, M.; Kato, K.; Adachi, K. The Difference in Running-in Period and Friction Coefficient between Self-Mated Si<sub>3</sub>N<sub>4</sub> and SiC Under Water Lubrication. *Tribol. Lett.* **2001**, *11*, 23–28. [\[CrossRef\]](#)
- Wang, S.; Cheng, J.; Zhu, S.; Qiao, Z.; Yang, J. Low friction properties of Ti<sub>3</sub>AlC<sub>2</sub>/SiC tribo-pair in sea water environment. *Tribol. Int.* **2016**, *103*, 228–235. [\[CrossRef\]](#)
- Wu, D.; Liu, Y.; Li, D.; Zhao, X.; Ren, X. The applicability of WC-10Co-4Cr/Si<sub>3</sub>N<sub>4</sub> tribo-pair to the different natural waters. *Int. J. Refract. Met. Hard Mater.* **2016**, *54*, 19–26. [\[CrossRef\]](#)
- Fischer, T.; Tomizawa, H. Interaction of tribochemistry and microfracture in the friction and wear of silicon nitride. *Wear* **1985**, *105*, 29–45. [\[CrossRef\]](#)
- Saito, T.; Hosoe, T.; Honda, F. Chemical wear of sintered Si<sub>3</sub>N<sub>4</sub>, hBN and Si<sub>3</sub>N<sub>4</sub>-hBN composites by water lubrication. *Wear* **2001**, *247*, 223–230. [\[CrossRef\]](#)
- Gao, Y.-M.; Fang, L.; Su, J.-Y.; Xie, Z.-G. Investigation on the components and the formation of a tribochemical film in the Si<sub>3</sub>N<sub>4</sub>-gray iron sliding pair lubricated with distilled water. *Wear* **1997**, *206*, 87–93. [\[CrossRef\]](#)
- Skopp, A.; Woydt, M.; Habig, K.-H. Tribological behavior of silicon nitride materials under unlubricated sliding between 22 °C and 1000 °C. *Wear* **1995**, *181-183*, 571–580. [\[CrossRef\]](#)
- Liu, N.; Wang, J.; Chen, B.; Yan, F. Tribochemical aspects of silicon nitride ceramic sliding against stainless steel under the lubrication of seawater. *Tribol. Int.* **2013**, *61*, 205–213. [\[CrossRef\]](#)
- Zhang, Z.; Li, X.; Almandoz, E.; Fuentes, G.G.; Dong, H. Sliding friction and wear behavior of Titanium-Zirconium-Molybdenum (TZM) alloy against Al<sub>2</sub>O<sub>3</sub> and Si<sub>3</sub>N<sub>4</sub> balls under several environments and temperatures. *Tribol. Int.* **2017**, *110*, 348–357. [\[CrossRef\]](#)
- Wang, C.; Ye, Y.; Guan, X.; Hu, J.; Wang, Y.; Li, J. An analysis of tribological performance on Cr/GLC film coupling with Si<sub>3</sub>N<sub>4</sub>, SiC, WC, Al<sub>2</sub>O<sub>3</sub> and ZrO<sub>2</sub> in seawater. *Tribol. Int.* **2016**, *96*, 77–86. [\[CrossRef\]](#)
- Skopp, A.; Woydt, M. Ceramic and Ceramic Composite Materials with Improved Friction and Wear Properties. *Tribol. Trans.* **1995**, *38*, 233–242. [\[CrossRef\]](#)
- Carrapichano, J.; Gomes, J.; Silva, R. Tribological behaviour of Si<sub>3</sub>N<sub>4</sub>-BN ceramic materials for dry sliding applications. *Wear* **2002**, *253*, 1070–1076. [\[CrossRef\]](#)

21. Chen, W.; Zhang, D.; Lv, Z.; Li, H. Self-lubricating mechanisms via the in situ formed tribo-film of sintered ceramics with hBN addition in a high humidity environment. *Int. J. Refract. Met. Hard Mater.* **2017**, *66*, 163–173. [[CrossRef](#)]
22. Chen, W.; Wang, K.; Gao, Y.; He, N.; Xin, H.; Li, H. Investigation of tribological properties of silicon nitride ceramic composites sliding against titanium alloy under artificial seawater lubricating condition. *Int. J. Refract. Met. Hard Mater.* **2018**, *76*, 204–213. [[CrossRef](#)]
23. Cho, M.; Kim, D.; Cho, W. Analysis of micro-machining characteristics of Si<sub>3</sub>N<sub>4</sub>-hBN composites. *J. Eur. Ceram. Soc.* **2007**, *27*, 1259–1265. [[CrossRef](#)]
24. Davim, J.P.; Cardoso, R. Effect of the reinforcement (carbon or glass fibers) on friction and wear behavior of the PEEK against steel surface at a long dry sliding. *Wear* **2009**, *266*, 795–799. [[CrossRef](#)]
25. Zhang, Z.; Breidt, C.; Chang, L.; Friedrich, K. Wear of PEEK composites related to their mechanical performances. *Tribol. Int.* **2004**, *37*, 271–277. [[CrossRef](#)]
26. Liao, W.J.; Nie, S.L.; Li, L.; Zhang, Z.H.; Yuan, S.H. Tribological Behavior of Carbon Fiber-reinforced PEEK Sliding against Engineering Ceramic SiC Lubricated with Seawater. *Chin. Hydraul. Pneum.* **2015**, *8*, 16–19. [[CrossRef](#)]
27. Chen, W.; Wang, Z.X.; Gao, Y.M.; Li, H.Q.; He, N.R. Microstructure, Mechanical Properties and Friction/Wear Behavior of Hot-Pressed Si<sub>3</sub>N<sub>4</sub>/BN ceramic composites. *Ceram.—Silik.* **2019**, *63*, 1–10. [[CrossRef](#)]
28. Chen, W.; Gao, Y.; Ju, F.; Wang, Y. Tribochemical Behavior of Si<sub>3</sub>N<sub>4</sub>-hBN Ceramic Materials with Water Lubrication. *Tribol. Lett.* **2010**, *37*, 229–238. [[CrossRef](#)]
29. Chen, W.; Wang, Z.; Liu, X.; Jia, J.; Hua, Y. Effect of load on the friction and wear characteristics of Si<sub>3</sub>N<sub>4</sub>-hBN ceramic composites sliding against PEEK in artificial seawater. *Tribol. Int.* **2020**, *141*, 105902. [[CrossRef](#)]
30. Bhushan, B.; Ko, P.L. *Introduction to Tribology*; John Wiley & Sons: New York, NY, USA, 2002.
31. Chen, W.; Gao, Y.; Chen, C.; Xing, J. Tribological characteristics of Si<sub>3</sub>N<sub>4</sub>-hBN ceramic materials sliding against stainless steel without lubrication. *Wear* **2010**, *269*, 241–248. [[CrossRef](#)]